JCI The Journal of Clinical Investigation

Morphologic alterations of the blood-brain barrier with experimental meningitis in the rat. Temporal sequence and role of encapsulation.

V J Quagliarello, … , W J Long, W M Scheld

J Clin Invest. 1986;77(4):1084-1095. https://doi.org/10.1172/JCI112407.

Research Article

The cerebral capillary endothelium is unique and functions as an effective blood-brain barrier (BBB) owing to its intercellular tight junctions and rare pinocytotic vesicles. To assess how bacterial meningitis alters the BBB, rats were inoculated intracisternally with three encapsulated meningeal pathogens (Escherichia coli K1+, Streptococcus pneumoniae type III, Haemophilus influenzae type b) and an unencapsulated mutant strain (H. influenzae Rd). After defined infection durations, the morphologic alterations of the cerebral capillary endothelium were quantitatively assessed by transmission electron microscopy. Results revealed a significant increase in pinocytotic vesicle formation (P less than 0.001) early after meningitis induction (4 h) that was sustained with longer infection durations (10 h, 18 h) for all encapsulated strains tested. In addition, there was a progressive increase in completely separated intercellular junctions with increasing infection duration, (P less than 0.05). 4 h after induction of meningitis with H. influenzae Rd, cerebrospinal fluid (CSF) bacterial concentrations, cerebral capillary morphologic changes, and functional BBB permeability to circulating 125I-albumin were similar to those observed with H. influenzae type b. However, prolonging the H. influenzae Rd infection to 18 h allowed for CSF clearance of the organism, thereby precluding the significant increase in separated junctions or progression of functional BBB permeability seen with the encapsulated H. influenzae type b. These data suggest a uniform morphologic explanation for altered BBB permeability […]

Morphologic Alterations of the Blood-Brain Barrier with Experimental Meningitis in the Rat

Temporal Sequence and Role of Encapsulation

Vincent J. Quagliarello, William J. Long, and W. Michael Scheld
Departments of Internal Medicine and Neurosurgery, University of Virginia School of Medicine, Charlottesville, Virginia 22908

Abstract

The cerebral capillary endothelium is unique and functions as an effective blood-brain barrier (BBB) owing to its intercellular tight junctions and rare pinocytotic vesicles. To assess how bacterial meningitis alters the BBB, rats were inoculated intracisternally with three encapsulated meningeal pathogens (*Escherichia coli* K1+, *Streptococcus pneumoniae* type III, *Haemophilus influenzae* type b) and an unencapsulated mutant strain (*H. influenzae* Rd). After defined infection durations, the morphologic alterations of the cerebral capillary endothelium were quantitatively assessed by transmission electron microscopy. Results revealed a significant increase in pinocytotic vesicle formation ($P < 0.001$) early after meningitis induction (4 h) that was sustained with longer infection durations (10 h, 18 h) for all encapsulated strains tested. In addition, there was a progressive increase in completely separated intercellular junctions with increasing infection duration, ($P < 0.05$). 4 h after induction of meningitis with *H. influenzae* Rd, cerebrospinal fluid (CSF) bacterial concentrations, cerebral capillary morphologic changes, and functional BBB permeability to circulating ^{125}I-albumin were similar to those observed with *H. influenzae* type b. However, prolonging the *H. influenzae* Rd infection to 18 h allowed for CSF clearance of the organism, thereby precluding the significant increase in separated junctions or progression of functional BBB permeability seen with the encapsulated *H. influenzae* type b. These data suggest a uniform morphologic explanation for altered BBB permeability in meningitis with a reproducible temporal sequence. Encapsulation does not appear essential for BBB injury, but may facilitate its progression by allowing the organism to evade host clearance.

Introduction

Bacterial meningitis remains a common disease with a high morbidity and mortality despite effective bactericidal antibiotic therapy (1). One hypothesis is that altered function of the blood-brain barrier (BBB)[1] secondary to infection in the subarachnoid space facilitates irreversible neuronal injury prior to, and despite, bacteriologic cure. Hence, defining the precise mechanism of infection-induced BBB injury is crucial to a better understanding of this disease.

Anatomically, investigations pioneered by Reese and Karnovsky (2) have localized the cerebral capillary endothelium as the major site responsible for the BBB. This is attributed to its unique characteristics as an endothelium compared with systemic capillaries. Systemic capillaries (i.e., those of glands and visceral mucosa) are fenestrated and allow intercellular passage of macromolecules and intact circulating cells; pinocytotic vesicular transport is common but mitochondria are rare. In contrast, cerebral capillaries exhibit rare pinocytosis, and the plasma membranes of adjacent endothelial cells are fused together in the form of continuous intact intercellular tight junctions, or zonulae occludentes (2, 3). This imparts on it the characteristics of a high-resistance endothelium (4, 5), and allows it to function as an effective barrier to macromolecular transport and cell exudation. Additionally, the high mitochondrial density of the cerebral endothelium (6) facilitates selective energy-dependent active transport of Na^+ and K^+ at the antiluminal membrane (7), and maintains homeostasis of the perineuronal interstitial fluid. Hence, only lipid-soluble substances or those transported by carrier-mediated diffusion (e.g., glucose, essential amino acids) traverse the BBB under normal circumstances (8–10).

Because the cerebrospinal fluid (CSF) is in direct continuity with the extracellular space bathing the cerebral capillaries, meningeal infection is a logical precipitant of BBB injury. This injury may consist of disruption of energy-dependent active transport systems, as well as barrier permeability arising from increasing pinocytosis or separation of tight junctions.

Despite decades of investigation of the BBB and its alteration with experimental injury, there remains a distinct paucity of data regarding its response to infection. In this investigation, we have developed a model of experimental meningitis in the rat to identify the natural history of the morphologic alterations induced in the BBB. Specifically our goals were: (*a*) to assess the influence of experimental bacterial meningitis on pinocytotic vesicle (PV) formation and intercellular junction integrity in the cerebral capillary endothelium using transmission electron microscopy; (*b*) to compare the morphologic changes seen with three encapsulated meningeal pathogens (*Streptococcus pneumoniae* type III, *Escherichia coli* K1+, *Haemophilus influenzae* type b)—all three possessing capsules of different composition;

This study was presented in part at the annual meeting of the American Federation for Clinical Research, Washington, DC, May 1985, and has appeared as an abstract (1985. *Clin. Res.* 33:416A).

Address reprint requests to Dr. Scheld, Division of Infectious Disease, Box 385, University of Virginia School of Medicine, Charlottesville, VA 22908.

Received for publication 20 May 1985.

J. Clin. Invest.

0021-9738/86/04/1084/12 $1.00
Volume 77, April 1986, 1084–1095

1. *Abbreviations used in this paper:* BBB, blood-brain barrier; cfu, colony-forming unit(s); CSF, cerebrospinal fluid; HRP, horseradish peroxidase; PRP, polyribosephosphate; PV, pinocytotic vesicle(s); SJ, separated junction(s); TJ, tight junction(s); WBC, white blood cell.

(*c*) to identify the temporal sequence of these morphologic changes by quantitating their appearance at infection durations (4, 10, and 18 h) that span the natural history of the disease; and (*d*) correlate the morphologic alterations in *H. influenzae* type b meningitis with functional BBB permeability to circulating ^{125}I-albumin, and contrast these changes with the morphologic and functional alterations induced by an unencapsulated mutant, *H. influenzae* Rd.

Methods

Challenge organisms. The encapsulated bacterial strains selected for study were carefully chosen to represent relevant human meningeal pathogens with different capsular compositions. The strain of *S. pneumoniae* type III used was derived from a clinical (CSF) isolate and has been previously characterized in this laboratory (11). 8-h late log phase organisms grown in trypticase soy broth (Difco Laboratories, Detroit, MI) supplemented with 5% defibrinated sheep blood at 37°C were centrifuged (250 *g* for 5 min to sediment erythrocytes), the supernatant recentrifuged (2,500 *g* for 15 min), the ensuing pellet washed in physiologic saline twice, and resuspended in 10 ml of 0.9% NaCl. The *E. coli* K1+ isolate (strain C94, kindly provided by Dr. G. McCracken, Dallas, TX) previously characterized in this laboratory, was grown to 8-h log phase in trypticase soy broth, centrifuged, washed, and resuspended as described above. The *H. influenzae* type b (Eagan) strain as well as the unencapsulated *H. influenzae* Rd mutant were obtained from the laboratory of E. Richard Moxon (Oxford University). Both *H. influenzae* strains were grown in brain-heart infusion broth, supplemented with 5% Fildes enrichment media (BBL Microbiology Systems, Cockeysville, Md.) and after an 8-h subculture of an overnight growth, were centrifuged, washed, and resuspended in phosphate-buffered saline. All final suspensions of challenge organisms were designed to achieve an inoculum of $10^{6.0-6.5}$ colony-forming units (cfu) in order to elicit a fatal meningitis. Log-phase organisms were used to facilitate maximal capsule expression in the challenge inocula.

Induction of meningitis. For the purpose of this investigation, it was necessary to develop a new model of experimental meningitis in the rat. Adult Wistar rats (150 g) were anesthetized with a combination of Ketamine (Parke-Davis, Morris Plains, NJ)/Xylazine (Miles Laboratories, Shawnee, KS) at a dose of 100 and 7 mg/kg, respectively, by the intramuscular route. 75 μl of CSF was removed via intracisternal puncture using a micromanipulator fitted to a 25-gauge butterfly needle (Abbott Inc., North Chicago, Ill.) calibrated for fluid increments of 25 μl. After removal of CSF, 50 μl of the challenge organism ($10^{6-6.5}$ cfu) was injected intracisternally into each experimental group, with 50 μl of saline (or phosphate-buffered saline) injected into simultaneous matched controls. Each experimental group consisted of at least three animals. After inoculation, meningitis was allowed to progress for defined durations (4, 10, and 18 h) and the CSF was resampled (75 μl) for determination of quantitative culture and white blood cell counts (WBC). Simultaneous blood samples were also obtained for quantitative cultures. 10-fold dilutions of CSF and blood were made in physiologic saline, and bacterial concentrations were determined by surface colony growth on blood agar (*S. pneumoniae* III, *E. coli* K1+) and chocolate agar (*H. influenzae* type b and Rd) plates. CSF WBC concentrations were determined with a hemocytometer by standard methods.

Cerebral capillary isolation. Immediately after confirmation of meningitis for each challenge organism at each time point (i.e., 4, 10, 18 h), the animals were killed by decapitation, and the intact brains were removed rapidly and placed in cold M199 media (Hank's salts, Gibco, Grand Island, NY) containing 20 mM Hepes, 100 U/ml penicillin, and 10 μg/ml streptomycin at pH 7.4. The meninges were removed with sterile paper tissue, and the brainstem, hindbrain, and choroid plexus were discarded using sterile instruments. The cerebral cortices from each experimental group were pooled in cold M199 media and minced with three pairs of sterile scissors, followed by homogenization with 20 strokes using a loose-fitting (0.25-mm clearance) homogenizer at 400 rpm after methods developed by Betz and Goldstein (8). The homogenate was diluted to 200 ml with M199 and centrifuged at 1,000 *g* for 10 min at 4°C. The supernatant was decanted, the pellets were resuspended by shaking for 60 s with 175 ml of 15% dextran (mol wt 60,000–90,000, Sigma Chemical Co., St. Louis, Mo.) in M199 media, and the suspension centrifuged at 4,000 *g* for 10 min at 4°C. The supernatant containing fat and dextran was discarded and the pellet containing cerebral capillaries resuspended in 10 ml of M199. The cerebral capillaries were collected on a 53-μm nylon mesh, washed with 150 ml of M199, and immediately fixed with 2% glutaraldehyde in 0.1 M phosphate buffer, pH 7.3.

Preparation for transmission electron microscopy. The fixed capillaries were washed three times, (5 min per wash) in 0.066 M phosphate buffer, pH 7.2, and centrifuged for 5 min at 4,000 *g*. Progressive dehydration was performed by rinsing samples in 40%, 60%, 80%, and 100% ethanol solutions, followed by further dehydration in a 1:1 solution of 100% ethanol/propylene oxide for 10 min, 100% propylene oxide for 10 min, and finally in a 1:1 solution of propylene oxide/epoxy resin (standard Epon 812 mixture) overnight. Subsequently, the capillaries were placed in 100% epoxy resin for 1 h, baked for 48–72 h in plastic capsules, and sectioned on an ultramicrotome (MT-5000 DuPont-Sorvall, Wilmington, DE). Multiple thin sections (~70 nm) were stained with 10% uranyl acetate and examined by transmission electron microscopy.

Horseradish peroxidase (HRP) visualization. The method used was a modification based on the procedure described by Graham and Karnovsky (12). To qualitatively assess HRP uptake into PV and penetration through separated intercellular junctions, selected experimental groups were injected 30 min prior to sacrifice with 60 mg type II HRP (Sigma Chemical Co.) intravenously, with the capillaries subsequently isolated as above. After fixation, the tissue was rinsed for 3 h at 0°C in several changes of 0.1 M phosphate buffer, pH 7.3, with 3.5% sucrose. The tissue was then incubated for 30 min at 25°C in 0.05% diamino-benzidine, tetra-HCl salt (Sigma Chemical Co.) in 0.1 M phosphate buffer, pH 6.0, followed by a 45-min incubation at 25°C in 0.05% diamino-benzidine in 0.1 M phosphate buffer, pH 6.0, with 0.01% H_2O_2. The capillaries were then rinsed in 0.1 M phosphate buffer, pH 7.3, at 0°C for 5–10 min and processed for transmission electron microscopy as above.

Quantitative analysis of the morphology of cerebral capillary endothelium. For each experimental and simultaneous control group, 30 random intact capillary cross-sections were quantitated blindly as to the number of PV, intact closed junctions, and separated junctions that were visualized. Separated junctions were defined as areas where plasma membranes of adjacent endothelial cells lining a capillary lumen were completely separated. Closed junctions were defined as areas where these adjacent membranes were continuously or partially joined. PV were defined as intact intracytoplasmic membrane-bound vesicles (70–180 nm); those incompletely forming at the luminal membrane or fusing with the antiluminal membrane were not quantitated. Only capillary sections <15 μm in diameter with intact luminal and antiluminal membranes were subjected to quantitative analysis. Because each thin section contained ≥50 capillary cross-sections, every effort was made to confine quantitation to the same thin section in order to avoid counting the same capillary section twice.

Quantitative functional assessment of BBB permeability to ^{125}I-bovine serum albumin (BSA). To correlate morphologic with functional alterations of the BBB, rats were injected intravenously with 10–20 μCi (0.15 ml) of ^{125}I-BSA (ICN Radiochemicals, Irvine, CA) ~30 min after intracisternal inoculation with *H. influenzae* type b and *H. influenzae* Rd. At the same time that CSF was sampled for quantitative culture, simultaneous blood and CSF samples were obtained, and radioactivity was measured directly in a Gamma 300 counter (Beckman Instruments, Inc., Irvine, CA). Only rats with clear CSF were used for measuring radioactivity. The percent CSF penetration was obtained by the following equation: counts per minute per milliliter of CSF/counts per minute per milliliter of blood × 100. The cerebral capillaries from these identical rats were then isolated and subjected to blinded quantitative analysis of PV formation and tight junction (TJ) integrity, as above.

Statistical analysis. The number of PV in experimental and control groups were compared using the Student t test (two-tailed unpaired). The proportion of junctions completely separated in experimental groups were compared with controls using the Fisher exact test (two-tailed). The mean percentage of ^{125}I-BSA penetration in experimental and control groups was compared using the Student t test (two-tailed, unpaired).

Results

Qualitative effects of experimental meningitis in the rat on the morphology of cerebral capillary endothelium: PV formation and TJ integrity

Morphologic assessment of PV formation by the cerebral capillary endothelium revealed a uniform host response to experimental meningitis with the encapsulated pathogens tested (*S. pneumoniae* type III, *E. coli* K1, *H. influenzae* type b). Namely, there was an increased cytoplasmic content of PV, visibly active formation at the luminal membrane, and demonstrable fusion of vesicles with the antiluminal membrane not seen in control preparations inoculated with saline. Depicted in Fig. 1 are examples of PV formation in cerebral capillary endothelium after 4 h of *E. coli* K1+ meningitis compared with a control preparation.

When alterations in the integrity of the intercellular junctions were assessed, a morphologic spectrum was recognized ranging from completely closed to completely separated with infection. Examples of typical intercellular junctional complexes visualized are depicted in Fig. 2. Fig. 2 *a* and *b* depict examples of completely separated intercellular junctions in rat capillaries after inoculation with *H. influenzae* Rd and *E. coli* K1+. Note that despite complete discontinuity in the encasement of the lumen by the endothelial cell layer, the luminal and antiluminal membranes are intact with little cytoplasmic rarefaction. A junctional complex that appears to be in transition (i.e., partially separated) is shown in Fig. 2 *c*, from a capillary cross section 18 h postinoculation with *E. coli* K1+. Evident is a junctional complex between adjacent endothelial cell membranes that is almost, but not completely, separated.

To qualitatively assess whether these morphologic changes were functionally significant, selected groups were injected intravenously 30 min prior to being killed with 60 mg of HRP (40,000 mol wt) to assess localization of a macromolecule the approximate size of albumin. As depicted in Fig. 3, after 18 h of experimental *E. coli* meningitis, one sees the presence of peroxidase activity within cytoplasmic vesicles as well as penetrating through a separated intercellular junction.

Quantitative effects of meningitis on PV formation and TJ integrity: temporal sequence

In order to compare quantitatively the degree of morphologic alterations induced, 30 random endothelial cell sections (≤15 μm in diameter) were examined blindly in each experimental (and its respective control) group. The number of intracytoplasmic PV and completely separated intercellular junction (SJ) were assessed and quantitated by blinded analysis 4, 10, and 18 h after inoculation.

E. coli K1+ meningitis. As shown in Fig. 4 *a*, a statistically significant increase in PV formation is noted as early as 4 h after inoculation with *E. coli* K1+ compared with saline-matched controls ([mean±SE] number of PV/100-nm capillary length, 5.57±0.57 vs. 2.76±0.37; $P < 0.001$). Although quantitatively greatest at 4 h, this increased PV formation remained significant at 10 h ($P < 0.02$) and 18 h ($P < 0.01$) postinoculation.

In contrast, the percentage of junctional complexes completely separated (representing the number of separated junctions per total number of junctions present in the same 30 capillary sections) increased with increasing infection duration, and reached statistical significance 10 h postinoculation. For example, 4 h postinoculation with *E. coli*, 9% of the junctional complexes (4/44) were completely separated as opposed to 0% (0/48) of controls ($P > 0.05$). However, when infection was allowed to progress for 10 h, 12% of junctions were separated (6/50) and were significantly increased ($P = 0.022$) when compared to controls (0/53). By 18 h postinoculation, the junctional separation with infection (10/54, 19%) reached greater significance ($P < 0.002$) compared to controls (0/51) (Fig. 4 *b*).

This temporal sequence of morphologic changes (i.e., early and sustained increase in PV formation, progressive increase in junctional separation) with increasing infection duration was associated with sustained CSF bacterial concentrations and WBC pleocytoses (Table I).

S. pneumoniae type III meningitis. Similar morphologic alterations of the cerebral capillary endothelium were noted after intracisternal inoculation with *S. pneumoniae* type III. As shown in Fig. 5 *a*, a statistically significant increase in PV formation as early as 4 h postinoculation with *S. pneumoniae* ([mean±SE] number of PV/100-nm capillary length, 6.38±0.67 vs. 2.76±0.37 in controls; $P < 0.001$) is evident. Although the mean number of PV per capillary section was quantitatively greatest at 4 h postinoculation, PV formation remained significantly increased when infection was allowed to progress for 10 h ($P < 0.05$) and 18 h ($P < 0.01$). Fig. 5 *b*, displaying the changes in intercellular junction integrity, demonstrates a similar increase in completely separated endothelial cell junctions that again reaches statistical significance 10 h postinoculation. That is, 4 h postinoculation with *S. pneumoniae* III, 7% (3/43) of the junctional complexes quantitated were completely separated as opposed to 0% (0/48) of controls ($P > 0.05$). However, when infection was allowed to progress for 10 h, 18% (10/56) of junctions were separated and were statistically increased ($P < 0.002$) compared to controls (0/53). Further progression of infection to 18 h showed that 17% (9/43) junctions separated, a value that again was highly statistically significant ($P < 0.003$) when compared to simultaneous saline-injected controls (0/51).

These morphologic changes were also associated with similar sustained CSF bacterial concentrations and WBC pleocytoses with increasing infection durations (Table II).

Correction of morphologic and functional alterations of the BBB in experimental H. influenzae meningitis. After confirming this remarkably similar temporal sequence of morphologic changes in the cerebral capillary endothelium with *E. coli* K1+ and *S. pneumoniae* type III meningitis, we contrasted the morphologic alterations induced by the encapsulated *H. influenzae* type b and the spontaneous unencapsulated mutant *H. influenzae* Rd.

As shown in Fig. 6, the sequence of morphologic changes seen with the encapsulated *H. influenzae* type b was similar to the other two encapsulated pathogens. Specifically, 4 h postinoculation with *H. influenzae* type b there was a statistically significant increase in PV formation compared with controls ([mean±SE] number of PV/100-nm capillary length, 5.24±0.52 vs. 2.72±0.35; $P < 0.001$). This increased PV formation with

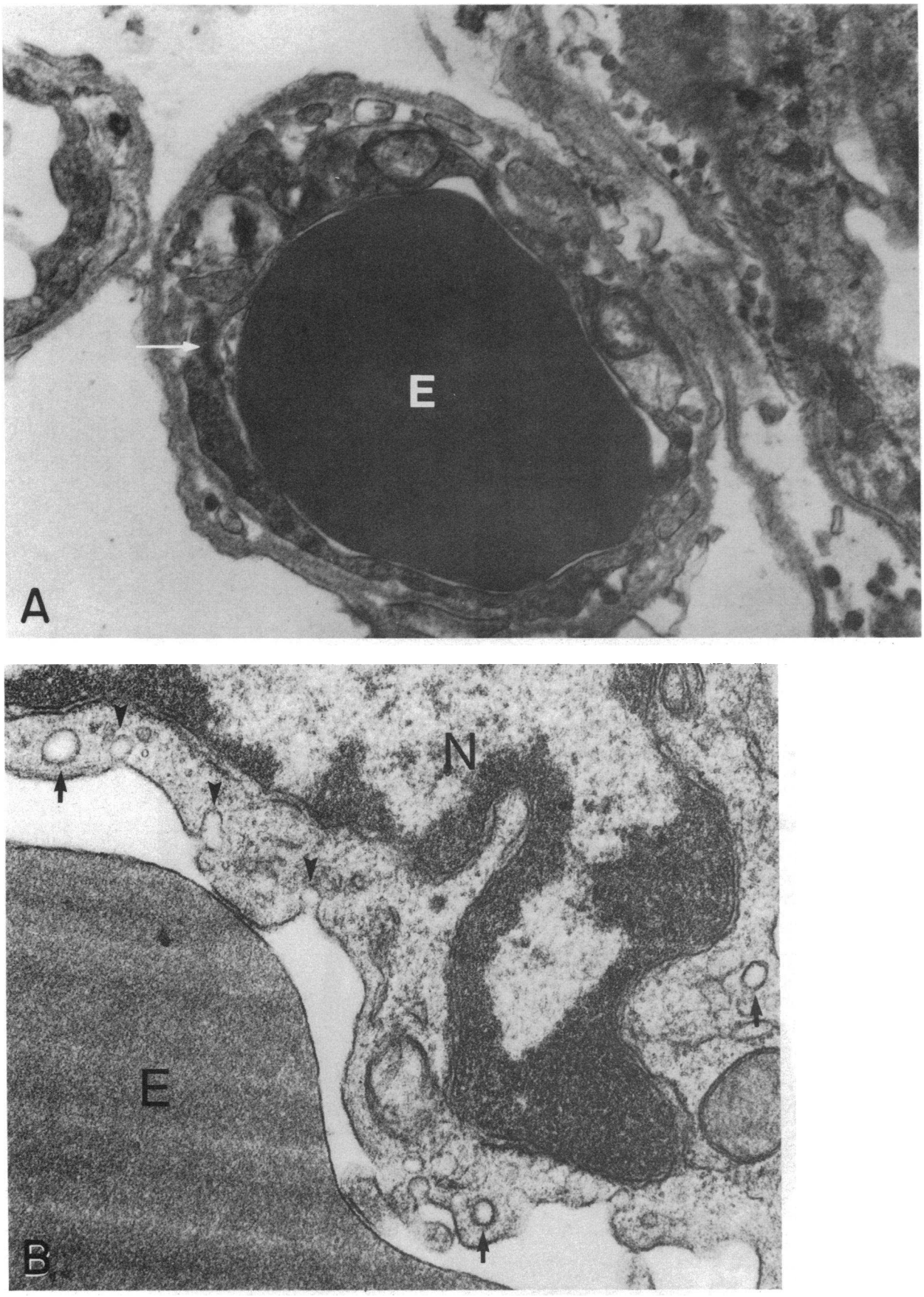

Figure 1. PV formation in cerebral capillary endothelium. (*A*) Control capillary cross section 18 h after saline inoculation. Note the visibly intact intercellular junction (*white arrow*) but the virtual absence of vesicles. *E*, intraluminal erythrocyte. × 15,000. (*B*) Capillary cross section 4 h postinoculation with *E. coli* K1+ showing vesicle formation at the luminal membrane (*arrowheads*) and within the cytoplasm (*arrows*). *E*, intraluminal erythrocyte; N, nucleus. × 60,000.

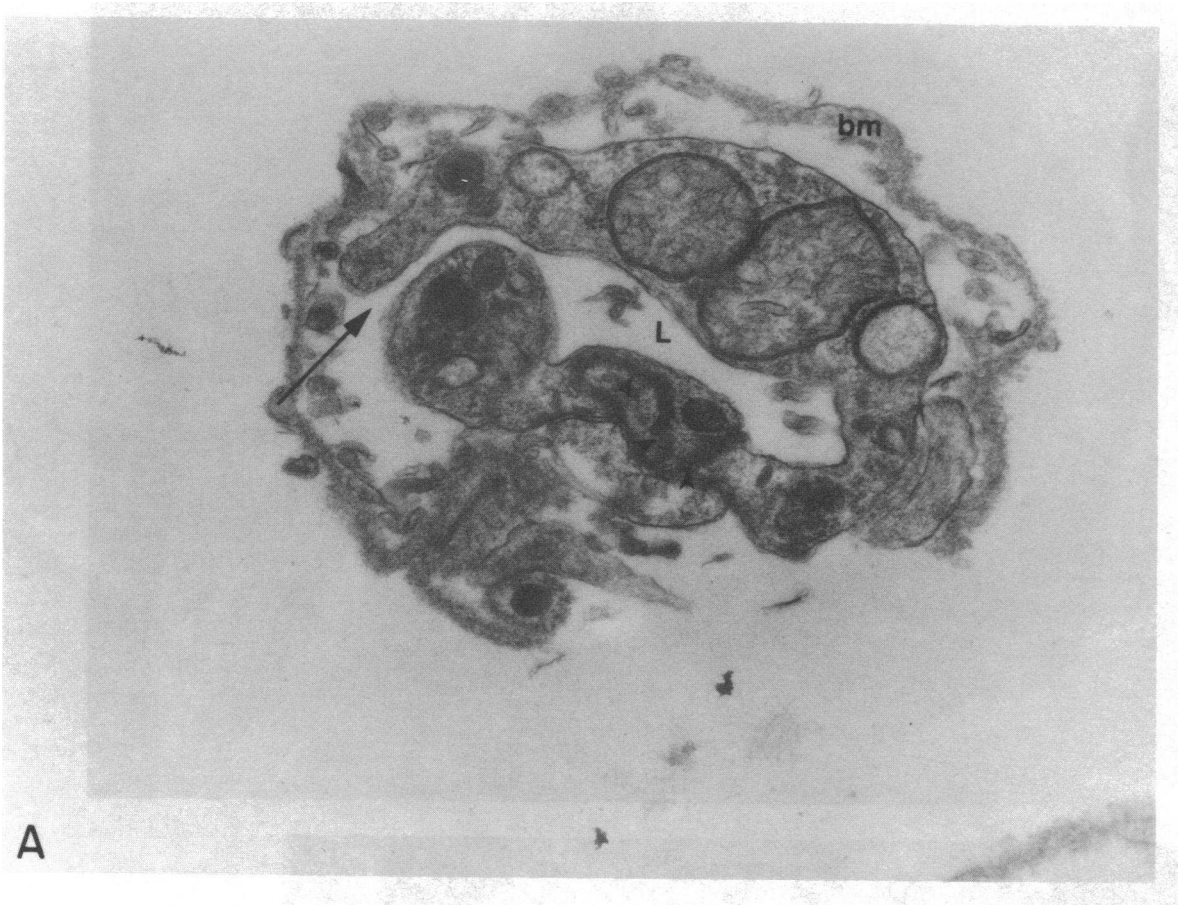
bm
L
A

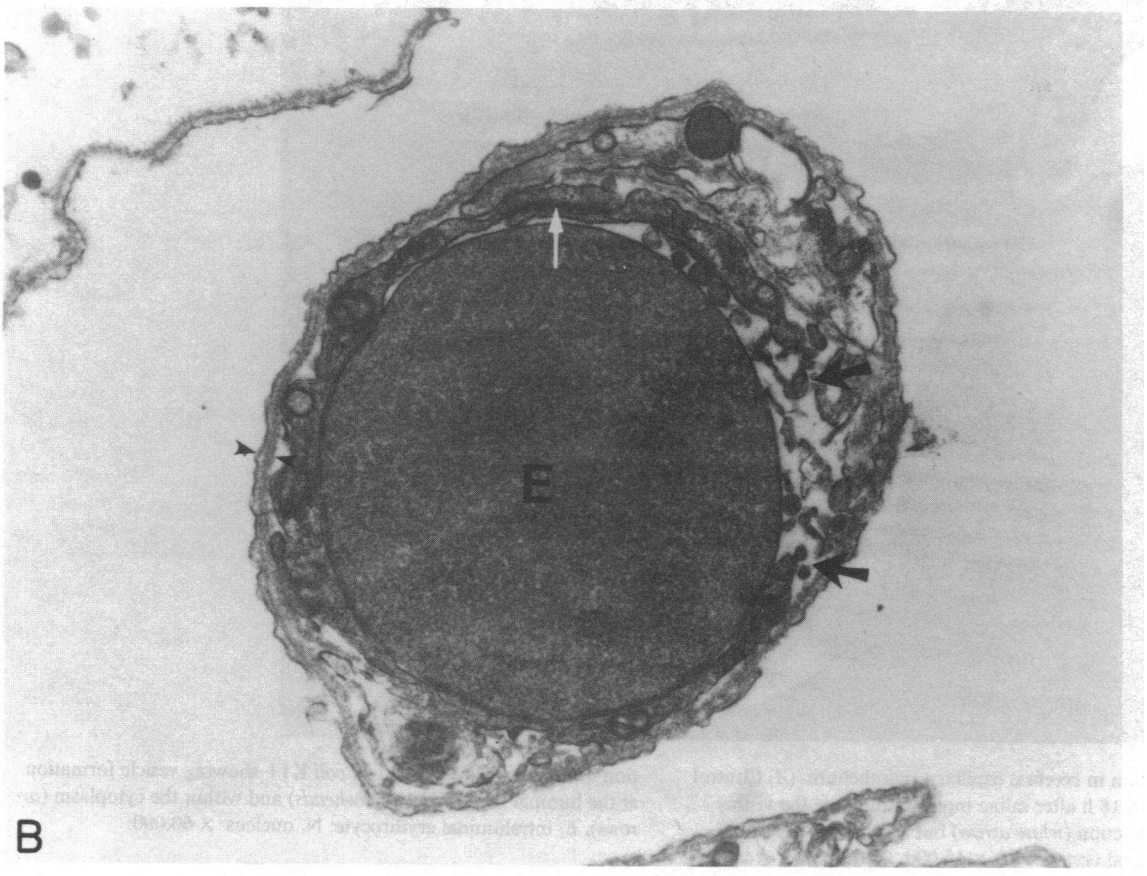
E
B

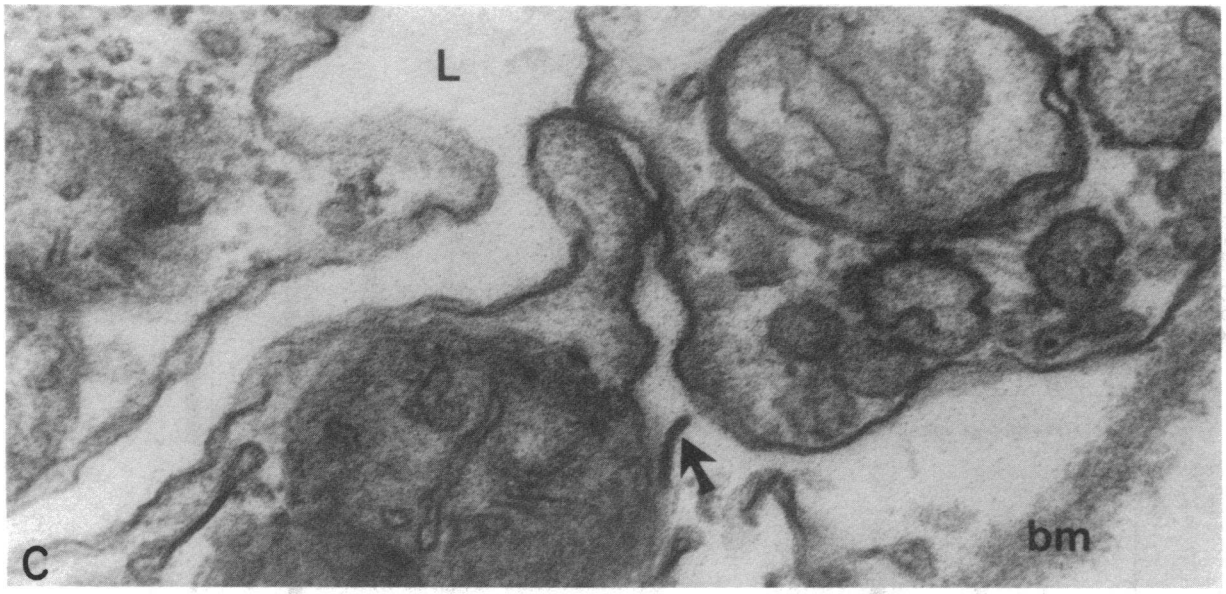

Figure 2. Morphologic alterations of intercellular junctions in cerebral capillary endothelium. (*Opposite*) (*A*) Capillary cross section 18 h postinoculation with *H. influenzae* Rd. Note the complete separation between adjacent endothelial cell membranes (*arrow*), which are otherwise continuously intact around the lumen (*L*). A visibly intact junction (*arrowheads*) is also present. Note the surrounding basement membrane (*bm*), which appears damaged by the infection (× 20,000). (*B*) Capillary cross section 4 h postinoculation with *E. coli* K1+. Note the wide separation between intact cell membranes of two endothelial cells (*black arrows*) that are otherwise joined by an intact intercellular junction (*white arrow*) at their other ends. Scattered cytoplasmic debris is present within the intercellular space but the basement membrane (*arrowheads*) is intact. *E*, erythrocyte (× 15,000.) (*Above*) (*C*) Capillary cross section 18 h postinoculation with *E. coli* K1+. Note the junctional complex (*arrow*) with a widened intercellular cleft but without complete separation; *bm*, basement membrane; *L*, lumen (× 30,000).

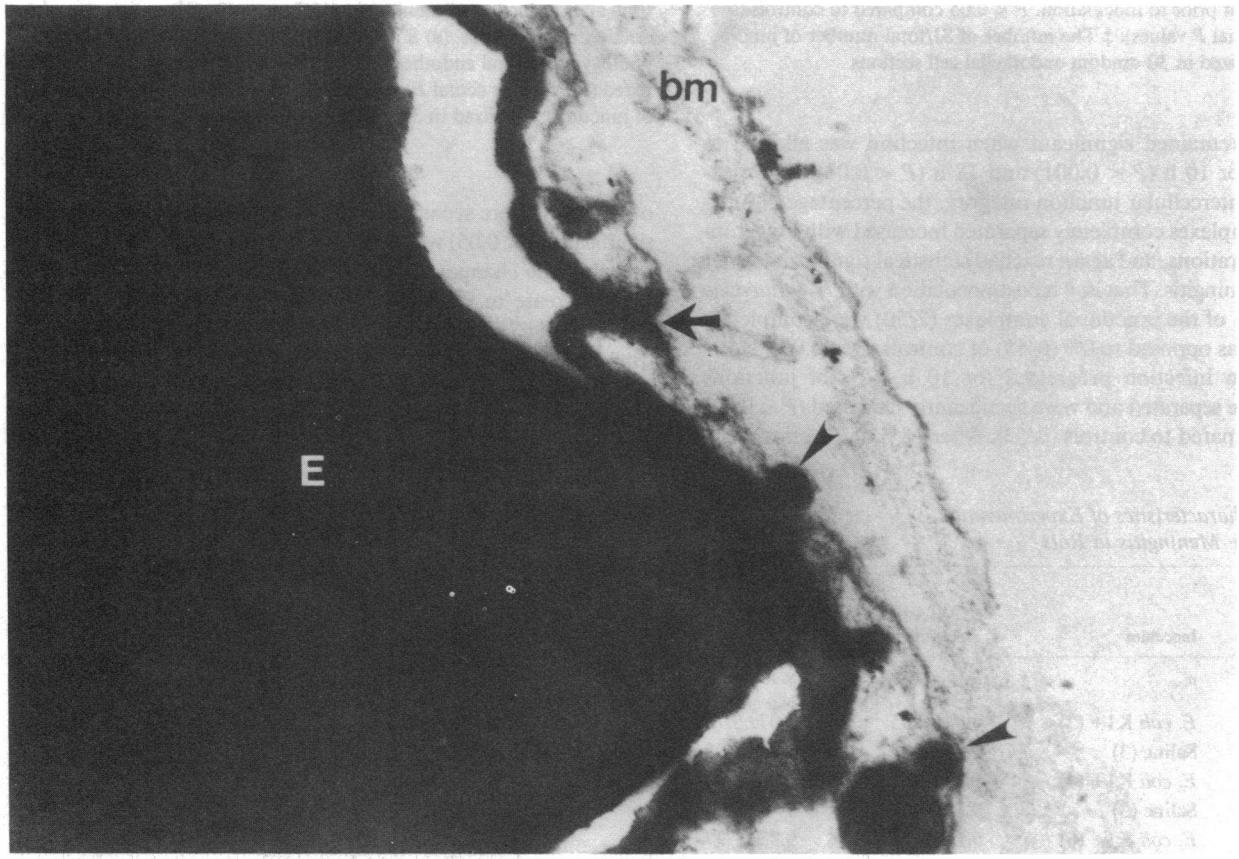

Figure 3. HRP visualization. Capillary cross section after 18 h of *E. coli* K1+ meningitis. Note the intracytoplasmic vesicles (150–180 nm) filled with peroxidase, including one that appears to be fusing with the antiluminal membrane (*arrowheads*). Moreover, note peroxidase product lining the endothelial lumen and penetrating through an intercellular junction (*arrow*). *E*, erythrocyte; *bm*, basement membrane (× 30,000).

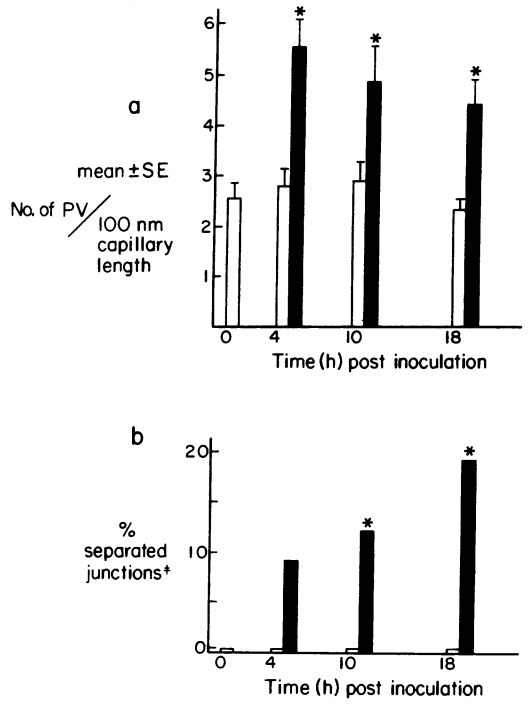

Figure 4. Morphologic changes in cerebral capillary endothelium with experimental *E. coli* K1+ meningitis. (*a*) PV formation vs. time after induction of meningitis. (*b*) Percent (%) SJ vs. time after induction of meningitis. (■) *E. coli;* (□) control; (time 0 □) morphology of cerebral endothelium prior to inoculation. $P < 0.05$ compared to controls (see text for actual P values). ‡ The number of SJ/total number of junctions visualized in 30 random endothelial cell sections.

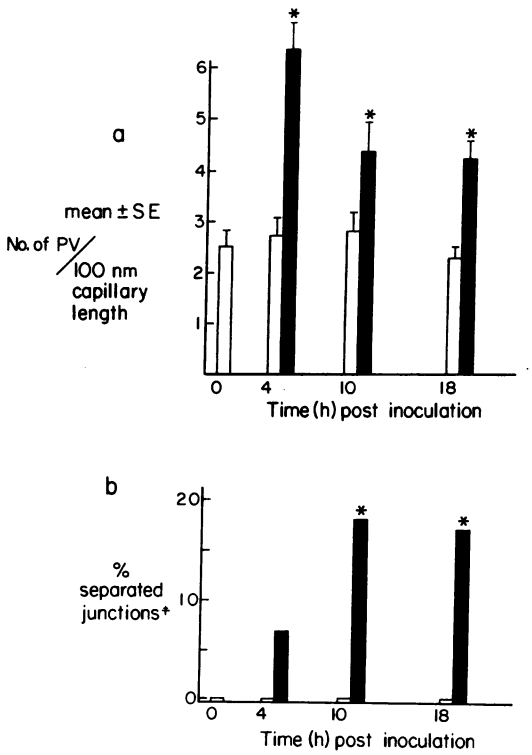

Figure 5. Morphologic changes in cerebral capillary endothelium with experimental *S. pneumoniae* type III meningitis. (*a*) PV formation vs. time after induction of meningitis. (*b*) Percent (%) SJ vs. time after induction of meningitis. (■) *S. pneumoniae;* (□) control; (time 0 □) morphology of cerebral endothelium prior to inoculation. $P < 0.05$ compared (see text for actual P values). ‡ The number of SJ/total number of junctions visualized in 30 random endothelial cell sections.

infection remained significant when infection was allowed to progress for 10 h ($P < 0.001$) and 18 h ($P < 0.01$). When examining intercellular junction integrity, the percentage of junctional complexes completely separated increased with longer infection durations, and again reached statistical significance after 10 h of meningitis. That is, 4 h postinoculation with *H. influenzae* type b, 4% of the junctional complexes (2/50) were completely separated as opposed to 0% (0/45) of controls ($P > 0.05$). However, when infection progressed for 10 h, 12% of junctions (7/58) were separated and were significantly increased ($P < 0.02$) when compared to controls (0/52). After 18 h of infection, 15% of junctions were separated (8/52) a difference which remained significant ($P < 0.05$) when compared with controls (1/46). These morphologic changes were associated with a statistically significant increase in CSF bacterial concentrations comparing the 4-h ([mean±SE] $\log_{10}$ cfu/ml of CSF, 6.26±0.34), with 18-h ([mean±SE] $\log_{10}$ cfu/ml, 8.06±0.35) infection ($P < 0.05$) (Table III). In addition, unlike the other two encapsulated pathogens, 100% of the animals were concomitantly bacteremic at all time

Table I. Characteristics of Experimental E. coli K1+ Meningitis in Rats

Duration of infection	Inoculum	CSF bacterial concentration*	WBC/ml of CSF
h	*n*	*$\log_{10}$ cfu/ml*	*× 10^3*
4	*E. coli* K1+ (3)	6.84±0.55	5.07±3.76
	Saline (3)	0	0.05±0.03
10	*E. coli* K1+ (4)	5.45±0.68	2.38±1.03
	Saline (3)	0	0
18	*E. coli* K1+ (6)	5.19±1.06	9.33±1.99
	Saline (6)	0	0.33±0.25

Values given as mean±SE.
* $P > 0.05$ comparing 4-, 10-, and 18-h CSF bacterial concentrations.

Table II. Characteristics of Experimental S. pneumoniae Type III Meningitis in Rats

Duration of infection	Inoculum	CSF bacterial concentration*	WBC/ml of CSF
h	*n*	*$\log_{10}$ cfu/ml*	*× 10^3*
4	*S. pneumoniae* (4)	6.28±0.18	3.11±2.39
	Saline (3)	0	0.05±0.03
10	*S. pneumoniae*	5.91±0.97	1.88±0.43
	Saline (3)	0	0
18	*S. pneumoniae* (4)	6.50±0.28	2.63±1.33
	Saline (6)	0	0.33±0.25

Values given as mean±SE.
* $P > 0.05$ comparing 4-, 10-, and 18-h CSF bacterial concentrations.

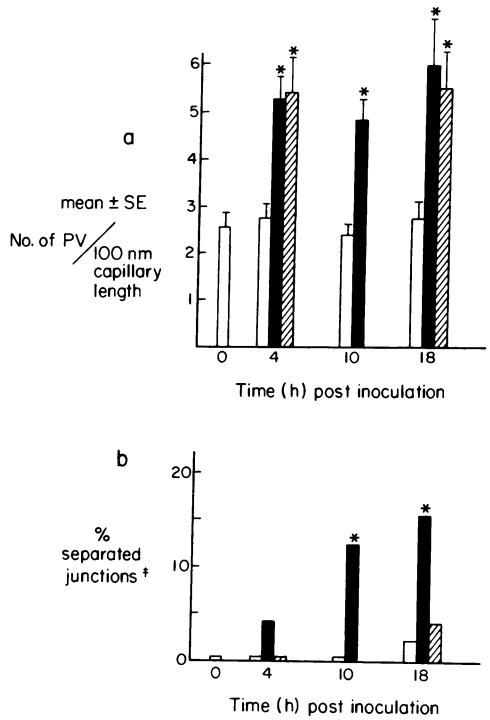

Figure 6. Morphologic changes in cerebral capillary endothelium with experimental *H. influenzae* type b and *H. influenzae* Rd meningitis. (*a*) PV formation vs. time after induction of meningitis (*b*) Percent (%) SJ vs. time after induction of meningitis. (■) *H. influenzae* type b; (▨) *H. influenzae* Rd; (□) control; (time 0 □) morphology of cerebral endothelium prior to inoculation. $P < 0.05$ compared to controls (see text for actual P values). ‡ The number of SJ/total number of junctions visualized in 30 random endothelial cell sections.

points with high bacterial concentrations (mean $\log_{10}$ cfu/ml blood > 4.0) (Table IV).

Functional correlation with the observed morphologic changes was obtained by assaying CSF penetration of ^{125}I-BSA at 4 and 18 h postinoculation. As shown in Table V, 4 h postinoculation with *H. influenzae* type b, there was a significant increase in ^{125}I-BSA penetration into CSF ([mean±SE] % ^{125}I-BSA penetration, 3.80±0.75) compared to controls (0.26±0.08; $P < 0.01$) that correlated with the observed increased PV formation. When infection progressed to 18 h there was a functional progression of ^{125}I-BSA permeability ([mean±SE] % ^{125}I-BSA penetration, 8.10±1.20) that was significantly greater than both the control group ([mean±SE] % ^{125}I-BSA penetration, 1.25±0.27; $P < 0.01$) as well as the 4-h *H. influenzae* type b infection ($P < 0.05$). This functional progression of albumin permeability correlated with the morphologic presence of both increased PV formation and the development of a statistically significant increase in SJ (Table V).

Comparison observations made after meningitis induced by *H. influenzae* Rd are depicted in Fig. 6 and Tables III and V. As shown, after receiving virtually identical inocula, there was no significant difference in CSF bacterial concentration (*P*

Table III. Characteristics of Experimental H. influenzae Type b vs. H. influenzae Rd Meningitis in Rats

Duration of infection	Inoculum	CSF bacterial concentration	WBC/ml of CSF
h	*n*	*$\log_{10}$ cfu/ml*	*× 10^3*
4	*H. influenzae* type b (4)	6.26±0.34	2.20±1.07
	H. influenzae Rd (3)	5.25±0.35*	4.02±1.69
	Saline (4)	0	0.01±0.01
10	*H. influenzae* type b (4)	7.88±0.39	0.63±0.63
	Saline (3)	0	0
18	*H. influenzae* type b (4)	8.06±0.35	2.56±0.51
	H. influenzae Rd (4)	3.32±0.32‡§	7.98±2.46
	Saline (3)	0	0.02±0.02

Values given as mean±SE.
* $P > 0.05$ compared with 4-h CSF *H. influenzae* type b concentration.
‡ $P < 0.01$ compared with 18-h CSF *H. influenzae* type b concentration.
§ $P < 0.05$ compared with 4-h CSF *H. influenzae* Rd concentration.

Table IV. Incidence and Magnitude of Bacteremia with Experimental Meningitis in the Rat

Challenge organism	Duration of infection	Proportion of animals bacteremic	Blood bacterial concentration
	h	%	*$\log_{10}$ cfu/ml*
E. coli K1+	4	2/3 (66)	1.25±0.74*
	10	1/4 (25)	0.43±0.42
	18	1/6 (17)	0.71±0.71
S. pneumoniae III	4	4/4 (100)	2.00±0.25
	10	4/4 (100)	1.33±0.12
	18	2/4 (50)	0.90±0.52
H. influenzae type b	4	4/4 (100)	4.77±0.08
	10	4/4 (100)	5.12±0.11
	18	4/4 (100)	4.53±0.35
H. influenzae Rd	4	0/3 (0)	0
	18	0/4 (0)	0

* Values given as mean±SEM.

Table V. Correlation of Morphologic and Functional Alterations of the BBB in H. influenzae Meningitis

	Inoculum	CSF bacterial concentration	CSF penetration of ^{125}I-albumin	Change in BBB morphology
	n	*$\log_{10}$ cfu/ml*	%	
4 h	Saline (3)	0	0.26±0.08	—
	H. influenzae Rd (3)	5.25±0.35	4.12±1.25*	↑ PV
	H. influenzae type b (4)	6.26±0.34	3.80±0.75*	↑ PV
18 h	Saline (4)	0	1.25±0.27	—
	H. influenzae Rd (4)	3.32±0.32§	4.64±0.80*	↑ PV
	H. influenzae type b (4)	8.06±0.35‡	8.10±1.20*‡	↑ PV + ↑ SJ

Values given as mean±SE.
* $P < 0.05$ compared to control.
‡ $P < 0.05$ compared to *H. influenzae* type b at 4 h and *H. influenzae* Rd at 18 h.
§ $P < 0.05$ compared to *H. influenzae* Rd at 4 h.

> 0.05), leukocyte count ($P > 0.05$), cerebral capillary morphology, or functional BBB penetration of ^{125}I-BSA when compared with *H. influenzae* type b 4 h postinfection. That is, there was a significant increase in PV formation ([mean±SE] number of PV/100-nm capillary length, 5.40±0.81 vs. 2.72±0.35; $P < 0.01$); but the percentage of SJ (0/46, 0%) was no different than controls (0/46). This correlated with a mean CSF ^{125}I-BSA penetration (4.21±1.26%) that was significantly greater than controls ($P < 0.05$) but no different than the functional penetration seen with *H. influenzae* type b at 4 h (3.80±0.75%). However, none of the animals with *H. influenzae* Rd meningitis were bacteremic at 4 h (Table IV), contrasting with 100% of those with *H. influenzae* type b meningitis.

When infection was allowed to progress for 18 h with *H. influenzae* Rd (Fig. 6), one sees a sustained increase in PV formation when compared with controls ($P < 0.01$) but, in contrast to *H. influenzae* type b, the percentage of SJ (2/47, 4%) did not quantitatively progress to reach statistical significance ($P > 0.05$) compared to controls (1/48, 2%). Similarly, functional penetration of ^{125}I-BSA was not significantly different 18 h postinoculation ([mean±SE] % ^{125}I penetration, 4.64±0.80) than it was 4 h postinfection ($P > 0.05$)—see Table V. This morphologic and physiologic distinction of *H. influenzae* Rd meningitis (when compared to *H. influenzae* type b) 18 h postinoculation, was associated with a significantly lower CSF bacterial concentration (mean $\log_{10}$ cfu/ml, 3.32) when compared with *H. influenzae* type b (mean $\log_{10}$ cfu/ml, 8.06; $P < 0.01$) despite identical inocula (Table III). The CSF WBC concentrations were not significantly different from *H. influenzae* type b; however, the absence of bacteremia with *H. influenzae* Rd was again distinctly different from the 100% incidence of high grade bacteremia noted with *H. influenzae* type b.

Discussion

In this investigation, we observed a uniform host response to experimental meningitis at the level of the cerebral capillary endothelium. Specifically, there was an early and sustained increase in PV formation as well as a progressive increase in separation of intercellular junctions observed during the natural history of the infection. Both morphologic changes appear to contribute to functional penetration of albumin across the BBB.

In the preantibiotic era, bacterial meningitis was a disease with devastating mortality claiming the lives of virtually all those afflicted (1). However, despite the advent of effective antimicrobial agents there remains a finite case fatality rate (e.g., 28% in *S. pneumoniae* meningitis) (13), with permanent neurologic sequelae affecting many survivors (14–16). One potential explanation is that the pathologic consequences of the disease beyond the leptomeninges, but within the central nervous system, progress despite bacteriologic cure (17). The BBB, the major portion of which is anatomically localized to the cerebral capillary endothelium, represents a critical extrameningeal site known to be functionally altered in meningitis (18–20). Although many critical functions of this unique endothelium (e.g., abluminal transport of Na^+ and K^+, carrier-mediated diffusion of hexoses and amino acids) are subject to injury, we sought to investigate the morphologic alterations rendering it more permeable during infection. Hence, we quantitatively assessed by transmission electron microscopy the morphologic changes in PV formation and intercellular junction integrity of the cerebral capillary endothelium using an experimental rat model of meningitis.

An in vivo model was developed for this investigation because morphologic and physiologic investigations suggest that permeability of the cerebral microvasculature is responsive to both neural (21, 22) and hormonal influence (23). Hence, any resultant change in its morphology and functional permeability might depend on a critical interaction between the inciting injury (e.g., infection), the inflammatory host response (e.g., PMN exudation), and humoral regulatory processes (e.g., adrenal cortical function, circulating catecholamines). Thus, an in vivo model possesses distinct advantages over in vitro techniques in facilitating this dynamic interplay. The cerebral microvasculature was chosen for morphologic assessment in this study because it represents the dominant site of the BBB. The circumventricular organs (e.g., choroid plexus, area postrema) theoretically contribute to the BBB despite fenestrations in their capillary supply because of the presence of epithelial tight junctions. However, the surface area of the cerebral microvasculature is 5,000-fold greater than the surface area of capillaries supplying the circumventricular organs (24, 25), rendering the former more pertinent for this investigation.

Qualitatively, our results revealed two distinct morphologic changes in the cerebral capillary endothelium resulting from meningeal infection. Namely, there was an increase in PV formation and complete separation of intercellular junctions that allowed for functional penetration of horseradish peroxidase to the abluminal side of the endothelium (Figs. 1–3). When these morphologic changes were quantitatively assessed by blinded analysis, a remarkably consistent temporal sequence was observed in meningitis induced by the encapsulated pathogens. For example, after intracisternal inoculation with *E. coli* K1+, there was a statistically significant increase in PV formation ($P < 0.001$) as early as 4 h later that was sustained when infection was allowed to progress for 10 h ($P < 0.02$) and 18 h ($P < 0.01$). Similar statistically significant increases in PV formation were observed soon after inoculation (i.e., 4 h) with the encapsulated *S. pneumoniae* type III as well as *H. influenzae* type b; these increases were likewise sustained when infection progressed for 10–18 h (Figs. 4–6). Hence, despite different capsule composition the morphologic alterations of PV formation were similar for all three encapsulated pathogens and correlated with sustained CSF bacterial concentrations and WBC pleocytosis (Tables I–III).

Transendothelial vesicular transport has been postulated as a potential mechanism of altered permeability of the BBB, although its significance remains conjectural. As previously noted, the cerebral capillary endothelium contains rare PV as opposed to systemic capillaries (e.g., muscle) in which they are abundant. In muscle capillaries, these vesicles have been shown to functionally endocytose and exocytose microperoxidase. The precise mechanism of transcellular vesicular transport is unknown but hypothesized to be either by Brownian motion of vesicles freely mobile in the cytoplasm, or via transcellular channels forming from transiently fused vesicles across the capillary wall (26). Hence, the unique paucity of vesicles within cerebral endothelium has been proposed as a potential contribution to its function as a barrier to macromolecular transport. Interestingly, other investigations have demonstrated qualitative increases in pinocytosis in brain endothelium after hypertensive (27), ischemic (28), and convulsive injury (29), but it remains unclear whether these are true quantitative and statistically significant increases. In our model of study, we are able to describe the precise onset of the insult (i.e., intracisternal inoculation of bacteria), the tem-

poral sequence of morphologic changes, and their quantitative functional significance regarding BBB permeability to various molecular weight proteins.

Morphologically, our data regarding increased cytoplasmic vesicular content during experimental meningitis could be interpreted in two ways. First, although luminal endocytosis is increased and cytoplasmic vesicular content increased, abluminal exocytosis may be nonexistent and hence functional transcellular transport insignificant. Indeed, investigations in a mouse model suggest that under normal conditions pinocytosed macromolecules by the cerebral capillary endothelium are destined for lysozomal fusion and degradation rather than abluminal exocytosis (30). Furthermore, these two critical processes necessary for vesicular transport (i.e., endocytosis and exocytosis) may be independently regulated (31); hence, the same injury to the endothelium may affect one without the other. However, one could also suggest that there could be greater luminal endocytosis than abluminal exocytosis resulting in a greater cytoplasmic vesicle content morphologically as well as functional transcellular protein transport. This interpretation is supported by the experiments with *H. influenzae* meningitis correlating the observed BBB morphologic changes with functional permeability to circulating ^{125}I-BSA. As shown (Fig. 6, Table V), 4 h postinoculation with *H. influenzae* type b and *H. influenzae* Rd when only cytoplasmic vesicular content was significantly increased, there was a significant increase in CSF penetration of ^{125}I-BSA ($P < 0.01$) compared with controls. Similarly, 18 h postinoculation with *H. influenzae* Rd when increased PV formation remained prominent (but junctional separation still insignificant) there was a similar quantitative CSF penetration of ^{125}I-BSA ([mean±SE] 4.64±0.80%) that remained significant ($P < 0.05$) compared with controls. Hence the morphologic appearance of increased PV formation appears to correlate with functional permeability of the BBB to circulating albumin suggesting that pinocytosis may be an independent mechanism of macromolecular transport in meningitis.

The temporal sequence of intercellular junction separation with experimental meningitis was distinctly different than that for PV formation, but was likewise reproducible regardless of the encapsulated pathogen tested. That is, a longer infection duration (10 h) of experimental meningitis was required for each encapsulated strain before the percentage of separated junctions reached statistical significance when compared to saline-matched controls. Furthermore, the percentage of separated junctions progressively increased with longer infection durations reaching a value of 17–19% at 18 h postinoculation (Figs. 4–6). Interestingly, however, is that despite the animals being clinically moribund 18 h after inoculation, the majority of the intercellular junctions visualized remained closed (i.e., <20% were separated). One explanation for this observation is that each junctional complex may vary in its degree of membrane fusion between adjacent endothelial cells. Hence, some junctions may be inherently "less tight" than others and thus more susceptible to separation upon infectious injury. This hypothesis is supported by freeze-fracture studies of epithelial tissue in which the TJ region was found to consist of a complex network of anastamosing linear strands appearing as ridges or grooves in the complementary fracture faces (32). The number and continuity of the anastomosing strands appeared to correlate with the transepithelial resistance (i.e., "tightness") of the tissue. For example, mammalian proximal convoluted renal tubule representing a weak barrier with a low electrical resistance (6 ohm-cm^2), had few or discontinuous anastomosing strands. In contrast, toad bladder epithelium, inherently tight physiologically (transepithelial resistance of 1,000–2,000 ohm-cm^2) had numerous anastamosing strands that were continuous. Hence, one could postulate that within the same capillary tissue preparation, although the resistance of junctional complexes are comparatively high (5), there may be variability among different capillaries as well as within the same capillary. Thus, given the same degree of injury, some junctions may completely separate while others may remain partially or completely intact.

A second possibility is that junctional separation may require a complex injury pattern and demand both luminal and antiluminal stress for completion. Hence, junctions found to separate in our studies may require not only antiluminal injury from bacterial surface ligands or extracellular toxins resultant from the meningitis. Simultaneous luminal injury from a sustained bacteremia or anoxic injury (perhaps from localized vasospasm) may be necessary contributing factors, and may be more severe in focal areas of the cerebral vasculature.

Supporting the hypothesis that junctional separation might require a complex injury pattern are our studies comparing morphologic and functional BBB alterations in *H. influenzae* type b vs. *H. influenzae* Rd meningitis (Tables IV and V; Fig. 6). The Rd strain was selected for comparison because it elaborates no detectable polyribosyl phosphate (PRP) capsule either by enzyme-linked immunosorbent assay (ELISA) or immunofluorescent techniques. Other spontaneous capsule-deficient mutants exist (e.g., S2 strain; Sec 1 strain) but both elaborate a finite, albeit small amount of PRP (4–45 ng/10^9 cells) (33). Hence, to assess whether BBB injury could occur despite absence of detectable capsule, the Rd strain was used for comparison. Ideally, one would desire a strain for comparison that possessed identical subcapsular surface components (e.g., outer membrane protein, lipopolysaccharide) to the encapsulated strain and differed only in its lack of encapsulation. Unfortunately, even genetically transformed strains (e.g., transformation of Rd strain with *H. influenzae* type b DNA) possess heterogeneous lipopolysaccharide patterns on sodium dodecyl sulfate-polyacrilamide gel electrophoresis that differ from the recipient (e.g., Rd) strain (34), precluding such a comparison at present.

As previously noted, when meningitis was induced with the Rd strain, identical morphologic changes of the cerebral capillary endothelium were noted (Fig. 6) when compared to *H. influenzae* type b 4 h after inoculation. Namely, there was an increased PV formation but no significant junctional separation. These changes correlated with significant CSF penetration of ^{125}I-albumin (Table V) and were present despite absence of detectable bacteremia with the Rd strain compared with the 100% incidence and high-grade bacteremia (mean±SE $\log_{10}$ cfu/ml, 4.77±0.08) seen 4 h postinoculation with *H. influenzae* type b (Table IV). These data suggest that increased vesicular transport as a host response to *H. influenzae* infection does not require the presence of either PRP capsule or bacteremia.

When meningitis was allowed to progress for 18 h with the Rd strain, the morphologic changes of the cerebral capillary endothelium remained the same (i.e., an increased PV formation but only 4% separated junctions; $P > 0.05$) and functional BBB permeability was unchanged (4.64% ^{125}I-BSA penetration) compared to the 4-h infection (4.12% ^{125}I-BSA penetration; $P > 0.05$). Again there was no detectable bacteremia and the CSF bacterial concentrations significantly decreased (compared to 4 h postinoculation) suggesting spontaneous host clearance of the unen-

capsulated strain. However, 18 h after inoculation with the encapsulated *H. influenzae* type b there was a significant increase in separated junctions (8/52, 15%) as well as sustained PV formation (Fig. 6); a phenomenon previously noted in the encapsulated *E. coli* K1+ and *S. pneumoniae* type III meningitis experiments. This development of a significant increase in separated junctions 18 h postinoculation was associated with a progression of BBB permeability to ^{125}I-BSA ([mean±SE] 8.1±1.2%) that was significantly greater than the permeability change induced by *H. influenzae* Rd at 18 h ($P < 0.05$) as well as *H. influenzae* type b at 4 h ($P < 0.05$)—see Table V. This morphologic progression (i.e., significant junctional separation) and increased functional BBB permeability were associated with a significant increase in the CSF bacterial concentration (compared with the 4-h CSF concentration) as well as the presence of a high-grade bacteremia (mean±SE $\log_{10}$ cfu, 4.53±0.35) in 100% of the animals. These observations suggest a role for the PRP capsule either as an independent effector of TJ injury or a factor facilitating high CSF and blood bacterial concentrations necessary for junctional separation. Different surface components (e.g., capsule, lipopolysaccharide, outer membrane proteins) may contribute independently or synergistically to the endothelial cell injury observed.

In summary, experimental meningitis in this model appears to elicit uniform morphologic alterations of the BBB with a reproducible temporal sequence. PV formation appears to be an early host response to infection in the subarachnoid space, followed by a progressive increase in complete separation of intercellular junctions as the infection progresses. Both morphologic host responses appear to contribute to functional alterations in BBB permeability to circulating macromolecules. Encapsulation as a neurovirulence factor for *H. influenzae* does not appear essential for morphologic or functional BBB injury but may facilitate their progression by allowing the organism to evade host clearance. Future investigation with this model will allow elucidation of the precise role of various bacterial surface components, the inflammatory host response, and intraluminal factors (e.g., local hypoxia, hormonal influences) in precipitating this injury.

Acknowledgments

The authors thank Dr. A. Lorris Betz (University of Michigan) for invaluable assistance with techniques for isolation of cerebral microvessels and Dr. John Povlishok (Medical College of Virginia) for review of the photoelectronmicrographs. Joyce Henderson prepared the manuscript.

This study was supported in part by a training grant (T32 AI07046) from the National Institutes of Health. Dr. Scheld is the recipient of a Clinical Investigator Award (K08-00517) from the National Institute of Allergy and Infectious Diseases and a research grant from the Thomas Jeffress and Kate Miller Jeffress Trust.

References

1. Swartz, M. N. 1984. Bacterial meningitis—more involved than just the meninges. *N. Engl. J. Med.* 311:912–914.

2. Reese, T. S., and M. J. Karnovsky. 1967. Fine structural localization of a blood brain barrier to exogenous peroxidase. *J. Cell Biol.* 34:207–217.

3. Brightman, M. W., and T. S. Reese. 1969. Junctions between intimately opposed cell membranes in the vertebrate brain. *J. Cell Biol.* 40:648–677.

4. Bradbury, M. W. 1984. The structure and function of the blood brain barrier. *Fed. Proc.* 43:186–190.

5. Crone, C., and S. P. Oleson. 1982. Electrical resistance of brain microvascular endothelium. *Brain Res.* 241:49–55.

6. Oldendorf, W. H., and W. J. Brown. 1975. Greater number of capillary endothelial mitochondria in brain than in muscle. *Proc. Soc. Exp. Biol. Med.* 149:736–738.

7. Betz, A. L., J. A. Firth, and G. W. Goldstein. 1980. Polarity of the blood brain barrier: distribution of enzymes between the luminal and antiluminal membranes of brain capillary endothelial cells. *Brain Res.* 192:17–28.

8. Betz, A. L., J. Csejtey, and G. W. Goldstein. 1979. Hexose transport and phosphorylation by capillaries isolated from rat brain. *Am. J. Physiol.* 236:C96–C102.

9. Betz, A. L., and G. W. Goldstein. 1978. Polarity of the blood-brain barrier: neutral amino acid transport into isolated brain capillaries. *Science (Wash. DC).* 202:225–227.

10. Goldstein, G. W., and A. L. Betz. 1983. Recent advances in understanding brain capillary function. *Ann. Neurol.* 14:389–395.

11. Scheld, W. M., and M. A. Sande. 1983. Bactericidal versus bacteriostatic antibiotic therapy of experimental pneumococcal meningitis in rabbits. *J. Clin. Invest.* 71:411–419.

12. Graham, R. C., and M. J. Karnovsky. 1966. The early stages of absorption of injected horseradish peroxidase in the proximal tubules of mouse kidney: ultrastructural cytochemistry by a new technique. *J. Histochem. Cytochem.* 14:291–302.

13. Centers for Disease Control. 1979. Bacterial meningitis and meningococcemia—United States, 1978. *Morbid. Mortal. Week. Rep.* 28: 277–279.

14. Alvon, V., V. Naveh, M. Gardos, and A. Greenman. 1971. Neurological sequelae of septic meningitis. *Isr. J. Med. Sci.* 15:512–517.

15. Ferry, P. C., J. L. Culbertson, J. A. Cooper, A. B. Silton, and S. H. W. Sell. 1982. Sequelae of *Haemophilus influenzae* meningitis: preliminary report of a long term follow-up study. *In Haemophilus influenzae:* Epidemiology, Immunology, and Prevention of Disease. S. H. Sell, and P. F. Wright, editors. Elsevier Biomedical, New York. 111–117.

16. Dodge, P. R., H. Davis, R. D. Feigen, S. J. Holmes, S. L. Kaplan, D. P. Jubelirer, B. W. Stechenberg, and S. K. Hirsh. 1984. Prospective evaluation of hearing impairment as a sequelae of acute bacterial meningitis. *N. Engl. J. Med.* 311:869–874.

17. Scheld, W. M., R. G. Dacey, H. R. Winn, J. E. Welsh, J. A. Jane, and M. A. Sande. 1980. Cerebrospinal fluid outflow resistance in rabbits with experimental meningitis: alterations with penicillin and methylprednisolone. *J. Clin. Invest.* 66:243–253.

18. Cooper, A. J., H. M. Beaty, S. I. Oppenheimer, C. J. Goodner, and R. G. Petersdorf. 1968. Studies on the pathogenesis of meningitis. VII. Glucose transport and spinal fluid production in experimental pneumococcal meningitis. *J. Lab. Clin. Med.* 71:473–481.

19. Spector, R., and A. V. Lorenzo. 1974. Inhibition of penicillin transport from the cerebrospinal fluid after intracisternal inoculation of bacteria. *J. Clin. Invest.* 54:316–325.

20. Prockop, L. D., and R. A. Fishman. 1968. Experimental pneumococcal meningitis: permeability influencing the concentration of sugars and macromolecules in cerebrospinal fluid. *Arch. Neurol.* 19:449–463.

21. Estrada, C., E. Hamel, and D. N. Krause. 1983. Biochemical evidence for cholinergic innervation of intracerebral blood vessels. *Brain Res.* 266:261–270.

22. Herbst, T. J., M. E. Raichle, and J. A. Ferrendelli. 1979. β-Adrenergic regulation of adenosine 3',5'-monophosphate concentration in brain microvessels. *Science (Wash. DC).* 204:330–332.

23. Long, J. B., and J. W. Holaday. 1985. Blood-brain barrier: endogenous modulation by adenal-cortical function. *Science (Wash. DC).* 227:1580–1583.

24. Pardridge, W. M. 1983. Neuropeptides and the blood-brain barrier. *Annu. Rev. Physiol.* 45:73–82.

25. Crone, C. 1971. The blood-brain barrier—facts and questions. *In* Ion Homeostasis of the Brain. B. K. Siesjo, and S. C. Sorenson, editors. Munksgaard, Copenhagen: 52–62.

26. Simionescu, N., M. Siminoescu, and G. E. Palade. 1978. Structural basis of permeability in sequential segments of the microvasculature of the diaphragm. II. Pathways followed by microperoxidase across the endothelium. *Microvasc. Res.* 15:17–36.

27. Westergaard, E. 1977. The blood brain barrier to horseradish peroxidase under normal and experimental conditions. *Acta Neuropathol.* 39:181–187.

28. Petito, C. K. 1979. Early and late mechanisms of increased vascular permeability following experimental cerebral infarction. *J. Neuropathol. Exp. Neurol.* 38:222–234.

29. Petito, C. K., J. A. Schaefer, and F. Plum. 1977. Ultrastructural characteristics of the brain and blood-brain barrier in experimental seizures. *Brain Res.* 127:251–267.

30. Broadwell, R. D., and M. Salcman. 1981. Expanding the definition of the blood-brain barrier to protein. *Proc. Natl. Acad. Sci. USA.* 78: 7820–7824.

31. Williams, S. K., and R. C. Wagner. 1981. Regulation of micropinocytosis in capillary endothelium by multivalent cations. *Microvasc. Res.* 21:175–182.

32. Claude, P., and D. A. Goodenough. 1973. Fracture faces of zonulae occludentes from "tight" and "leaky" epithelia. *J. Cell Biol.* 58:390–400.

33. Zwahlen, A., J. A. Winkelstein, and E. R. Moxon. 1983. Participation of complement in host defense against capsule deficient *Haemophilus influenzae. Infect. Immun.* 42:708–715.

34. Zwahlen, A., J. A. Winkelstein, and E. R. Moxon. 1983. Surface determinants of *Haemophilus influenzae* pathogenicity: comparative virulence of capsular transformants in normal and complement-depleted rats. *J. Infect. Dis.* 148:385–394.